International Journal of Control and Automation
Vol. 10, No. 1 (2017), pp.85-98
http//dx.doi.org/10.14257/ijca.2017.10.1.08

Decoupling Control Strategy of BLIM Based on Neural Network Inverse System

Wenshao Bu, Ziyuan Li, Juanya Xiao and Xiaoqiang Li

Information Engineering College, Henan University of Science and Technology, Luoyang, 471023, China
wsbu@163.com

Abstract

BLIM, i.e. bearingless induction motor, is a multi-variable, nonlinear and strong coupling object. To achieve its high performance control, a combined control strategy based on voltage control type neural network inverse system is proposed. In order to take the stator current's dynamics into account, the stator voltage components are selected as the input variables of torque system, the inverse system model of torque system is trained and identified by neural network, and witch is used to decouple the torque system into two second order linear subsystems. On this basis Based, the negative feedback control of radial displacement components, and the compensation of unbalance unilateral electromagnetic pull components are achieved in magnetic suspension control system; for the convenience of decoupling calculation of magnetic suspension system, the required air gap flux-linkage of torque system is identified online. The proposed combined control strategy is verified by system simulation. When the proposed control strategy is adopted, reliable decoupling between rotor flux-linkage, motor speed and two radial displacement components can be achieved; compared with the decoupling control strategy based on analytic inverse system, the control system owns stronger dynamic response characteristics and stronger ability of anti disturbance. The proposed control strategy is effective feasible.

Keywords: *Three-phase bearingless induction motor; Dynamics of stator current; Voltage control type; Neural network inverse System; Combined control strategy*

1. Introduction

Conventional AC motor supported by mechanical bearing has been widely used in industrial production [1], but it is difficult to meet the requirement of long time and high-speed operation; then the AC motor supported by magnetic bearing is developed and widely used [2-4], but it still has some disadvantages, such as more power consumption of magnetic suspension, over speed difficulty, *etc* [2], [4-7]. Bearingless motor is a new type of AC motor that is proposed based on the comparability in structure between magnetic bearing and conventional AC motor [5, 8, 9]. In bearingless motor, there are two sets of windings, include torque windings (with pole-pairs p_1 and current angular frequency ω_1), and suspension control windings (with pole-pairs p_2 and current angular frequency ω_2); The suspension magnetic field that caused by suspension control windings, would break the balance and symmetry of the conventional motor's revolving magnetic field, and results in magnetic field enhancement in some air-gap area, and weakening in the symmetrical area in space. The radial resultant force of additional Maxwell electromagnetic fore would be in the direction of the enhanced magnetic field. When the two sets of windings meet the conditions of "$p_1 = p_2 \pm 1, \omega_1 = \omega_2$", by the interaction of air gap flux-linkages produced by two sets of windings, the controllable magnetic suspension force can be produced, and it can be used to support the bearingless rotor [5]. Taking

ISSN: 2005-4297 IJCA

four-pole bearingless induction motor with two-pole suspension control windings as an example, Figure 1 shows the production principle of magnetic suspension force. When the currents are injected in two sets of windings as shown in Figure 1, the magnetic field in upper part of motor air gap is enhanced, and that in lower part of motor air gap is weaken, the resultant radial electromagnetic force, *i.e.* magnetic suspension force would be produced along β direction; If the current direction of suspension control windings is reversed, the resultant radial electromagnetic force would be produced along anti β direction. The production principle of magnetic suspension force along α reference axes is similar to this.

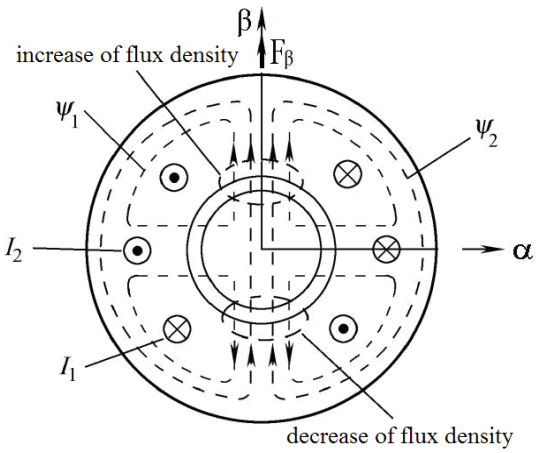

Figure 1. Production Principle of Magnetic Suspension Force

Bearingless induction motor owns many merits, such as robust structure, higher reliability, no wear and no need of lubrication. And then it is one of the most promising bearingless motor.

But bearingless induction motor is a multi-variable, nonlinear and strong coupling object; there exists complex electromagnetic coupling relationship inside; then to achieve its high performance control, it is necessary to achieve the dynamic decoupling between relevant variables [10, 11]. The differential geometry method and inverse system method are often used to decouple the complex object. But, the differential geometry method often solves relevant problem in the geometric domain, the mathematical operation is complex [12]. Inverse system method is achieved by nonlinear feedback and linearization, its physical concept is clear; but the accurate inverse system model of bearingless motor is complex also [10, 13, 14]. Neural network can approximate the complex nonlinear function with arbitrary precision, and has the self learning ability; it can be used to control the bearingless motor. In reference [15] and [16], neural network is used to identify the inverse system model of bearingless induction motor, and an idea is provided for the neural network inverse system control of bearingless induction motor; but the presented inverse model ignores the dynamics of stator current.

In the paper, the four-pole bearingless induction motor with two-pole suspension control windings is taken as the research object; a combined control strategy based on neural network inverse system is proposed. To improve its dynamic control performance of bearingless induction motor, the stator current's dynamics of torque system is taken into account, and then based on neural network inverse system method; the dynamic decoupling control between rotor flux-linkage and motor speed is achieved firstly. Then on the basis of this, the negative feedback control of radial displacement components, and the compensation of unbalance unilateral magnetic pull components are achieved in magnetic suspension system. System simulation has verified the validation of the proposed control strategy.

2. Mathematical Model of Bearingless Induction Motor

2.1. Mathematical Model of Two-Pole Suspension System

Defining *dq* as the synchronous coordinate system oriented by rotor flux linkage of four-pole torque system. Ignoring the weaker mutual inductance coupling between two sets of windings, the controllable magnetic suspension force components along horizontal α direction and vertical β direction can be expressed as follows[10]:

$$F_\alpha = K_m(i_{s2d}\psi_{1d} + i_{s2q}\psi_{1q}) \tag{1}$$

$$F_\beta = K_m(i_{s2d}\psi_{1q} - i_{s2q}\psi_{1d}) \tag{2}$$

In equations (1) and (2): F_α and F_β are controllable magnetic suspension force components along α and β directions; ψ_{1d} and ψ_{1q} the air gap flux linkage components along *d* and *q* coordinate axes; i_{s2d} and i_{s2q} are the suspension control current components along *d* and *q* coordinate axes; K_m is the magnetic force coefficient determined by the structure of bearingless induction motor.

According to the mechanical dynamics principle, the suspension motion equations of bearingless rotor can be expressed as follows:

$$m\ddot{\alpha} = F_\alpha + f_\alpha \tag{3}$$

$$m\ddot{\beta} = F_\beta + f_\beta \tag{4}$$

Hereinto, *m* is the mass of bearingless rotor; f_α and f_β are the unilateral magnetic pull components along α and β directions, witch are caused by the unbalanced distribution of air gap magnetic field when bearingless rotor deviates from the stator's center. The expressions of f_α and f_β are as follows:

$$f_\alpha = k_s\alpha, \quad f_\beta = k_s\beta \tag{5}$$

Hereinto, parameter k_s is the stiffness coefficient of radial displacement, witch is determined by the structure of bearingless induction motor; α and β are radial displacement components of bearingless rotor.

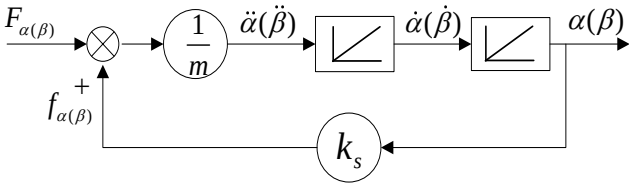

Figure 2. Suspension Motion Schematic Diagram of Bearingless Rotor

Figure 2 shows the suspension motion principle of bearingless rotor. It can be seen that the suspension motion of bearingless rotor is unstable. To achieve the suspension control of bearingless rotor, it is necessary to adopt negative feedback closed-loop control for radial displacement components.

2.2. Mathematical Model of Four-Pole Torque System

The torque production principle of bearingless induction motor's torque is the same with common induction motor. Ignoring the influence of suspension magnetic field on the magnetic field of torque system, and taking the stator current dynamics into account, the dynamic model of torque system can be expressed as follow [10]:

$$\frac{di_{s1d}}{dt} = -\frac{R_{s1}L_{r1}^2 + R_{r1}L_{m1}^2}{\sigma L_{s1}L_{r1}^2} i_{s1d} + \omega_1 i_{s1q} + \frac{L_{m1}\psi_{r1}}{\sigma L_{s1}L_{r1}T_{r1}} + \frac{u_{s1d}}{\sigma L_{s1}} \tag{6}$$

$$\frac{di_{s1q}}{dt} = -\omega_1 i_{s1d} - \frac{R_{s1}L_{r1}^2 + R_{r1}L_{m1}^2}{\sigma L_{s1}L_{r1}^2} i_{s1q} - \frac{L_{m1}\omega_r \psi_{r1}}{\sigma L_{s1}L_{r1}} + \frac{u_{s1q}}{\sigma L_{s1}} \tag{7}$$

$$\frac{d\psi_{r1}}{dt} = -\frac{\psi_{r1}}{T_r} + \frac{L_{m1}i_{s1d}}{T_{r1}} \tag{8}$$

$$\frac{d\omega_r}{dt} = \frac{p_1^2 L_{m1}\psi_{r1}i_{s1q}}{JL_{r1}} - \frac{p_1 T_L}{J} \tag{9}$$

In equations (6)~(9): i_{s1d} and i_{s1q} are the stator current components of torque windings along d and q coordinate axes; ψ_{r1} is the rotor flux-linkage of torque system; ω_r is the rotational angular velocity of rotor; L_{m1} is the mutual inductance of equivalent two-phase torque winding in dq coordinate system; L_{s1} is the self-inductance of equivalent two-phase torque winding in dq reference axis, $L_{s1}=L_{m1}+L_{s1l}$; L_{s1l} is the leakage inductances of stator windings; L_{r1} is the self-inductance of equivalent two-phase rotor winding in dq coordinate system, $L_{r1}=L_{m1}+L_{r1l}$; L_{r1l} is the leakage inductances of rotor windings; R_{r1} is the rotor resistance; T_{r1} is the time constant of rotor; T_L is the load torque.

The air gap flux-linkage is required in the decoupling control of magnetic suspension system. It can be got according to the relationship between rotor flux-linkage and air gap flux-linkage. The phase and amplitude of rotor flux linkage can be expressed as follows:

$$\varphi = \int (p_1\omega_r + L_{m1}i_{s1q}/T_{r1}\psi_{r1}) \tag{10}$$

$$\psi_{r1} = L_{m1}i_{s1d}/(T_{r1}s+1) \tag{11}$$

Then the air gap flux linkage of torque system in dq coordinate system can be expressed as follow:

$$\psi_{1d} = L_{m1}(\psi_{r1} + L_{r1l}i_{s1d})/L_{r1} \tag{12}$$

$$\psi_{1q} = L_{m1}L_{r1l}i_{s2q}/L_{r1} \tag{13}$$

3. Neural Network Inverse Decoupling Control of Torque System

3.1. Reversibility Analysis of Torque System under the Condition of Considering Stator Current Dynamics

To take the stator current dynamics into account, the stator voltage components of torque windings should be taken as the input variables, as shown in equation (8).

$$u = (u_1, u_2)^T = (u_{s1d}, u_{s1q})^T \tag{8}$$

At the same time, the state variables and output variables are selected as follows:

$$x = (x_1, x_2, x_3, x_4)^T = (i_{s1d}, i_{s1q}, \psi_{r1}, \omega_r)^T \tag{9}$$

$$y = (y_1, y_2)^T = (\psi_{r1}, \omega_r)^T \tag{10}$$

Put equations (8) ~ (10) into equations (6) ~ (9), the state equations of torque system that considers the stator current dynamics can be derived as follows:

$$\dot{x}_1 = -(\gamma-\delta)x_1 + (p_1x_4 + L_{m1}\delta x_2/x_3)x_2 + \xi\delta\eta x_3 + \xi u_1 \tag{11}$$

$$\dot{x}_2 = -(\gamma-\delta)x_2 - (p_1x_4 + L_{m1}\delta x_2/x_3)x_1 - p_1\xi\eta x_3x_4 + \xi u_2 \tag{12}$$

$$\dot{x}_3 = L_{m1}\delta x_1 - \delta x_3 \tag{13}$$

$$\dot{x}_4 = \mu x_2x_3 - p_1T_L/J \tag{14}$$

Relevant coefficients are as follows:

$$\gamma = \frac{R_{s1}}{\sigma L_{s1}} + \frac{R_{r1}}{\sigma L_{r1}},\ \sigma = 1 - \frac{L_{m1}^2}{L_{s1}L_{r1}},\ \delta = \frac{R_{r1}}{L_{r1}},\ \xi = \frac{1}{\sigma L_{s1}},\ \mu = \frac{p_1^2 L_{m1}}{JL_{r1}},\ \eta = \frac{L_{m1}}{L_{r1}}.$$

By means of interactor algorithm, the reversibility of torque system that considers the stator current dynamics can be analyzed. The output variables $y=(y_1,y_2)^T$ should be asked the derivative to time gradually, until the input variable $u_j(j=1,2)$ is obviously included in the derivative functions of each $y_i(i=1,2)$. The detail solving steps can be expressed as follows:

$$\dot{y}_1 = L_{m1}\delta x_1 - \delta x_3 \tag{15}$$

$$\ddot{y}_1 = L_{m1}\delta[-(\gamma-\delta)x_1 + (p_1x_4 + L_{m1}\delta x_2/x_3)x_2 + \xi\delta\eta x_3 + \xi u_1] - \delta^2\ (L_{m1}x_1 - x_3) \tag{16}$$

$$\dot{y}_2 = \mu x_2 x_3 - \frac{p_1}{J}T_L \tag{17}$$

$$\ddot{y}_2 = \mu x_3[-(\gamma-\delta)x_2 - (p_1x_4 + L_{m1}\delta x_2/x_3)x_1 - p_1\xi\eta x_3x_4 + \xi u_2] + \mu\delta x_2(L_{m1}x_1 - x_3) \tag{18}$$

Assumption: $Y=[\ddot{y}_1,\ddot{y}_2]^T$. There is following Jacobi matrix:

$$A(x,u) = \frac{\partial Y}{\partial u} = \begin{bmatrix} \delta\xi L_{m1} & 0 \\ 0 & \mu\xi x_3 \end{bmatrix} \tag{19}$$

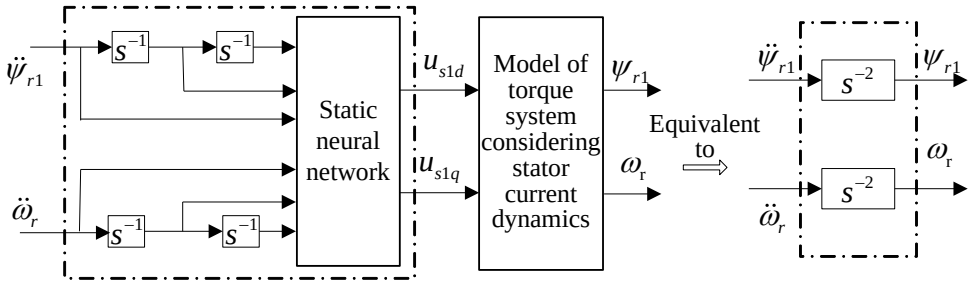

Figure 3. Pseudo Linear Composite System Composed of Neural Network Inverse System and Torque System

In normal operation, the rotor flux linkage doesn't equal to zero, *i.e.* $x_3=\psi_{r1}\neq 0$, then $\det(A)=\mu\delta\xi^2 x_3 \neq 0$, $rank(A)=2$. The Jacobi matrix $A(x,u)$ is non singular. The relative order $\alpha=[\alpha_1,\alpha_2]^T=[2,2]^T$, the sum of relative order equals to 4, *i.e.* equals to the order of torque system. Then according to the inverse system theory, it can be known that the torque system that considers the stator current dynamics is reversible.

3.2. Voltage control type Neural Network Inverse System Decoupling of torque system

Under the condition of considering the stator current dynamics, the inverse system model of torque system oriented by rotor flux-linkage can be expressed as follow [10]:

$$u = \phi(\ddot{y}_1, \dot{y}_1, y_1, \ddot{y}_2, \dot{y}_2, y_2) \tag{20}$$

Here, static neural network and attached integrators are adapted to construct voltage control type neural network inverse system model of torque system. Static neural network is used to characterize the nonlinear mapping relationship of inverse system; the attached integrators are used to characterize the dynamic characteristics of inverse system; and by adjusting the weights of static neural network, the identification of inverse system model can be achieved. By series connecting the neural network inverse system in front of the original torque system, then the torque system can be compensated to a pseudo linear system witch includes two linear subsystems, *i.e.* a second order linear integral rotor flux-linkage subsystem and a second order linear integral motor speed subsystem, as shown in Figure 3.

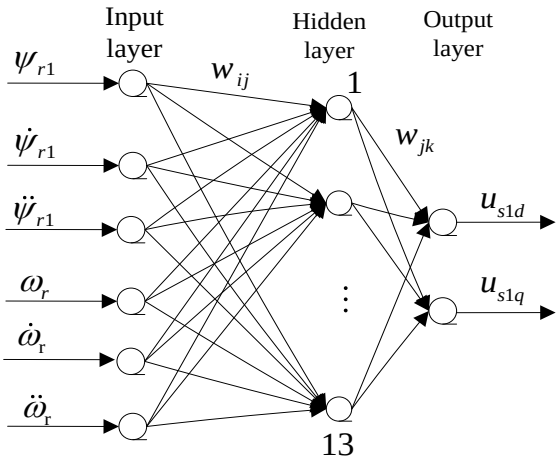

Figure 4. Three Layer Feedforward Static Neural Networks

In the inverse system identification process, a three layer feedforward static neural network is adopted; its topological structure is shown in Figure 4. There are three input nodes in input layer, two output nodes in output layer, and thirteen nodes in the hidden layer. A hyperbolic tangent type S transfer function is used as the excitation function of hidden layer neuron, as shown in equation (21).

$$f(x) = \frac{\exp(x) - \exp(-x)}{\exp(x) + \exp(-x)} \tag{21}$$

The output layer is composed with several neurons that own linear threshold excitation function. After the structure of neural network inverse system is determined, based on the training sample set, and adopting adequate learning algorithm, the neural network inverse system model is learned and trained offline, until the training error is small enough and the neural network inverse system of controlled object is derived.

The training process of neural network inverse system model can be summed up as the follows:

(1) Firstly, obtaining training sample set from the analytic inverse system of bearingless induction motor. Here the adopted analytic inverse system has taken the stator current dynamics into account [10]. Using the normal distribution random signal as the given signal of rotor flux linkage, whose amplitude is within the range from 0.45 Wb to 0.9Wb; using the normal distribution random signal as the given signal of motor speed, whose amplitude is within the range from zero to 3000r/min. The duration of given signals should be long enough, so that all the dynamic and stable information of system response can be included in the sampled datum. In the paper, the given signal of rotor flux linkage and that of motor speed are continued 0.7s and 1.1s respectively. Taking 0.005s as the sampling step, within the total excitation time of 30s, the rotor flux linkage, motor speed and the two voltage components of torque windings are sampled. Figure 5 shows the sampled original datum that is used to train neural network inverse system.

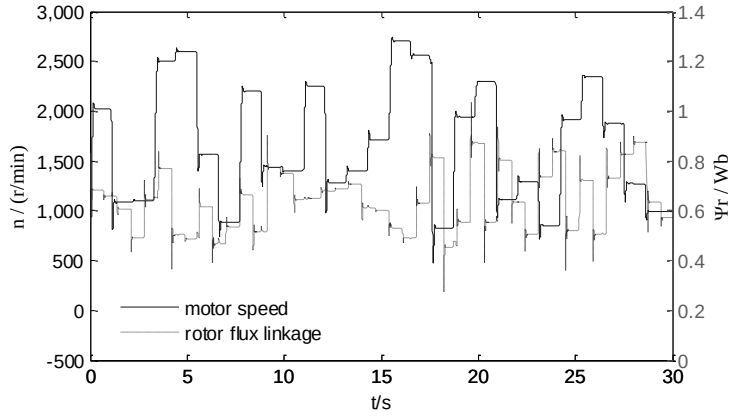

(a) Sampled data of rotor flux linkage and motor speed

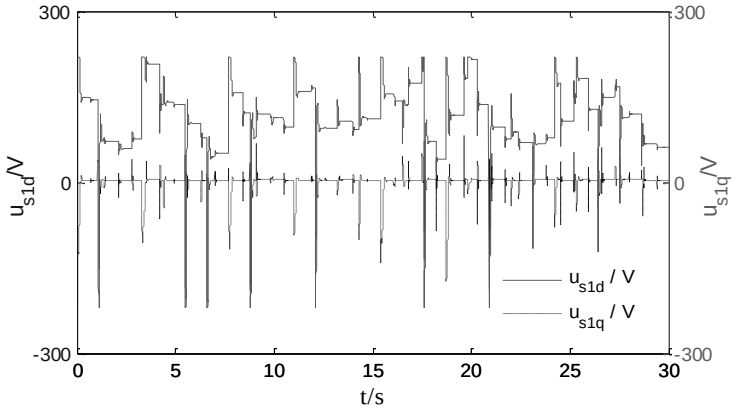

(b) Sampled data of stator voltage components

Figure 5. Sampled Original Data that Is Used To Train Neural Network Inverse System

(2) Constructing training sample set of neural network. After the sampled datum are smoothing filtered, based on five bit numerical differential method, the first and second order derivatives of rotor flux linkage and motor speed are derived, then the training sample set $\{\ddot{\psi}_{r1}, \dot{\psi}_{r1}, \psi_{r1}, \ddot{\omega}_r, \dot{\omega}_r, \omega_r\}$ and $\{u_{s1d}, u_{s1q}\}$ is constructed. From the sampled 6000 groups of datum, selecting 4000 groups as training set, the left 2000 groups are used as test set. In the practical application, the sampled raw data and the derivative data obtained from numerical differential treatment may not be in an order of magnitude, the training sample sets should be normalized to be within the range from -1 to +1. The normalization of training sample sets is good for convergence of neural network training, and the problem that neural network is too sensitive or not sensitive to some input variable, can be avoided.

(3) Adopting genetic algorithms to optimize the initial weights and thresholds of BP neural network, so that the BP neural network can approximate the analytic equation of nonlinear inverse system in equation (20). The basic idea of optimization can be summarized as follows: using the individual in genetic algorithm to represent the initial weights and thresholds of neural network; after the individual values of BP neural network are initialized, using the norm of BP neural network's prediction error as the fitness value, then by selection, cross connection and variation operations, the best weights and thresholds of neural network can be obtained.

(4) At the end, adopting LM algorithm, the static neural network should be trained based on the optimized initial weights and thresholds. After about 1000 times of training, the output's mean square error of neural network would be less than 0.001, then each

weight coefficient of static neural network can be determined, and the neural network inverse system of torque system can be achieved.

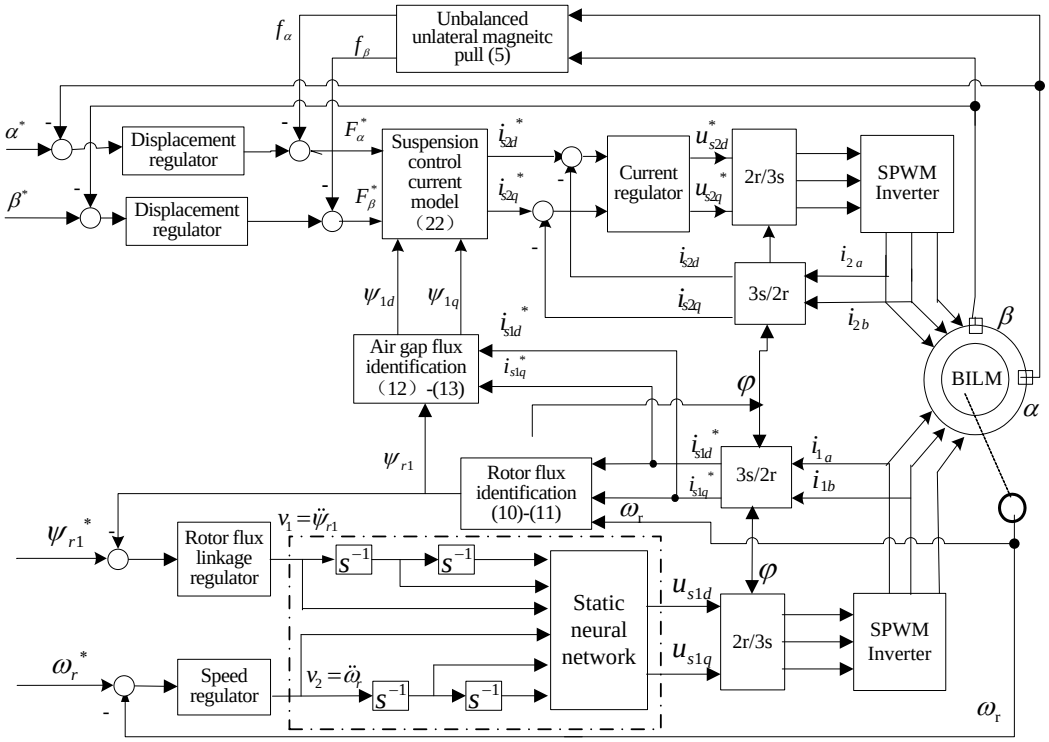

Figure 6. Control System Structure of Bearingless Induction Motor Based On Voltage Control Type Neural Network

4. Control System of Bearingless Induction Motor

Figure 6 gives the decoupling control system structure. Hereinto, the voltage control type neural network inverse system decoupling strategy is used for torque system; for magnetic suspension system, the radial displacement feedback control and feedforward compensation strategy of unbalanced unilateral magnetic pull are adopted.

4.1. Neural Network Inverse Decoupling Control of Torque System

Series connecting the trained neural network inverse system in front of the original torque system, the torque system can be decoupled into two second order linear integral subsystems, includes motor speed subsystem and rotor flux linkage subsystem, as shown in Figure 3; then adopting additional linear closed loop controller, the torque system can be effectively controlled. After neural network inverse decoupling, the transfer functions of motor speed and rotor flux linkage subsystems are "G(s) =1/s2". In order to get a good control effect, according to linear control theory, PD controllers are selected as the regulators of motor speed subsystem and rotor flux linkage subsystem.

For the influence of stator current dynamics has been taken into account, after the neural network training, more accurate neural network inverse model of torque system can be obtained; at the same time, for the voltage components along d and q coordinate axes are selected as the input variables of torque system, then the stator current's closed loop regulation can be omitted in the original torque system, and then the control system structure can be simplified in a certain degree.

4.2. Radial Displacement Feedback Control and Unbalanced Force Compensation

To achieve the stable suspension control of unbalanced rotor, PID regulators are used for the negative feedback control of radial displacement components; after the outputs of regulators are compensated with the unbalanced unilateral magnetic pull components, the given signals of controllable magnetic suspension force F_α^* and F_β^* can be derived.

From equations (1) and (2), it can be seen that the magnetic suspension force components derive from the interaction between the air gap magnetic field of torque system and the suspension control current. As long as the air gap flux linkage components ψ_{1d} and ψ_{1q} be calculated online according to equations (12) and (13), then according to the required signals of controllable magnetic suspension force components, *i.e.* F_α^* and F_β^*, the control current components i_{s2d} and i_{s2q} can be calculated online. The analytical formulas of magnetic suspension control current components can be expressed as follows:

$$\begin{pmatrix} i_{s2d}^* \\ i_{s2q}^* \end{pmatrix} = \frac{1}{K_m(\psi_{1d}^2+\psi_{1q}^2)} \begin{pmatrix} \psi_{1d} & \psi_{1q} \\ \psi_{1q} & -\psi_{1d} \end{pmatrix} \begin{pmatrix} F_\alpha^* \\ F_\beta^* \end{pmatrix} \tag{22}$$

5. System Simulation and Analysis

Figure 6 shows the control system of bearingless induction motor. To verify the proposed control strategy, taking a four-pole bearingless induction motor with two-pole suspension winding as the controlled object, system simulation has been made by Matlab/Simulink. The parameters of prototype bearingless induction motor are shown in Table.1.

Setting simulation conditions: Initial radial displacements of bearingless rotor: α_0=-0.12mm, β_0= -0.16mm; given value of stator flux-linkage: ψ^*_{s1}= 0.95*Wb*; Initial given value of rotational speed: n^*= 1500 *r/min* (*i.e.* ω_r^*=157rad/s); given signals of radial displacement components α^*=β^*=0. The motor starts with no-load; to analyze the decoupling control performance, the given signals of motor speed, rotor flux-linkage, and two radial displacement components are suddenly changed at different time.

Table 1. Parameters of Bearingless Induction Prototype Motor

parameters	*Description*	*Value*
r	Stator inner diameter (mm)	62
l	effective core length (mm)	82
δ_1	air gap of auxiliary bearing (mm)	0.2
P	Power of motor (kW)	2.2
R_s	stator winding resistance (Ω)	1.6
R_r	rotor winding resistance (Ω)	1.423
L_{s1l}	leakage inductance of torque windings (H)	0.0043
L_{r1l}	leakage inductance of rotor windings of torque system (H)	0.0043
L_{m1}	mutual inductance of torque system (H)	0.0859
J	rotation inertia of motor (kg.m^2)	0.024
R_{s2}	Suspension stator winding resistance	2.7
L_{s2l}	leakage inductance of suspension stator windings (H)	0.00398
L_{m2}	mutual inductance of suspension system (H)	0.230

Figure 7 ~ Figure 10 gives the response curves of control system. For the convenience of comparison, the response curves of analytical inverse decoupling control system are given also [10]. In the figures, the dotted lines are response curves of analytical inverse

decoupling control system, the solid lines are response curves of the proposed combined control method based on voltage control type neural network inverse system decoupling. From Figure 7 ~ Figure 10, there are following conclusions:

1) In the no-load starting stage, compared with analytical inverse system decoupling control method, when the proposed combined control method is adopted, the motor speed and rotor flux linkage can reach their stable values more quickly, their overshoots are obviously smaller, and the two radial displacement components own quicker response speed. Simulation results have shown the better starting performance of the proposed combined control strategy.

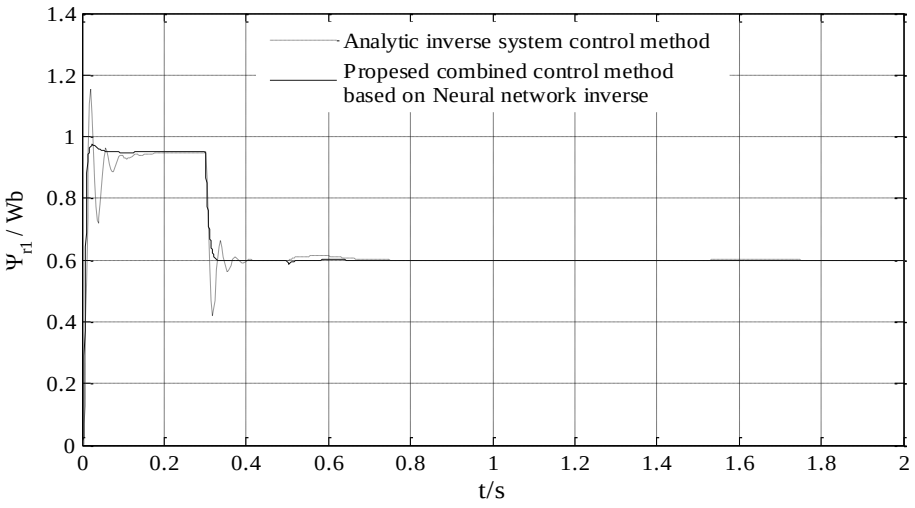

Figure 7. Response Curve of Rotor Flux Linkage

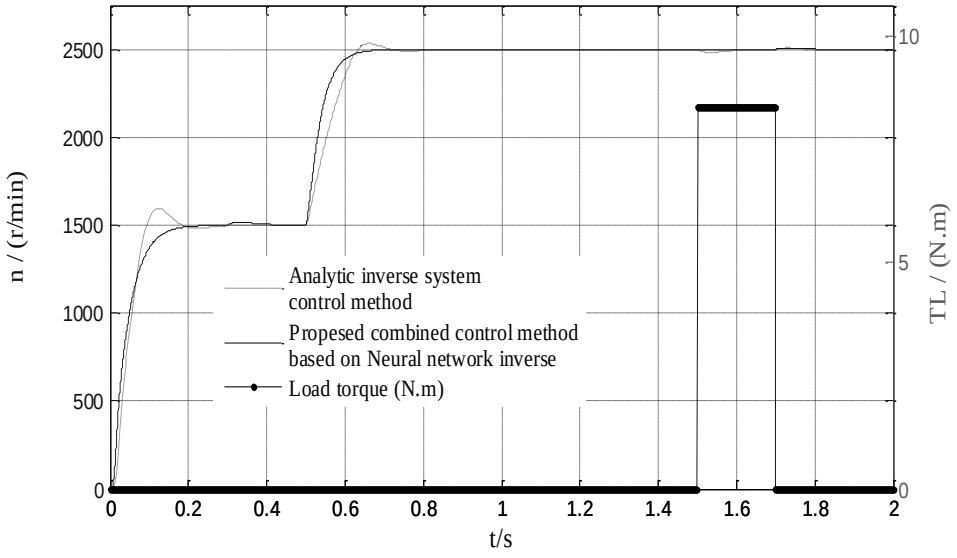

Figure 8. Response Curve of Motor Speed

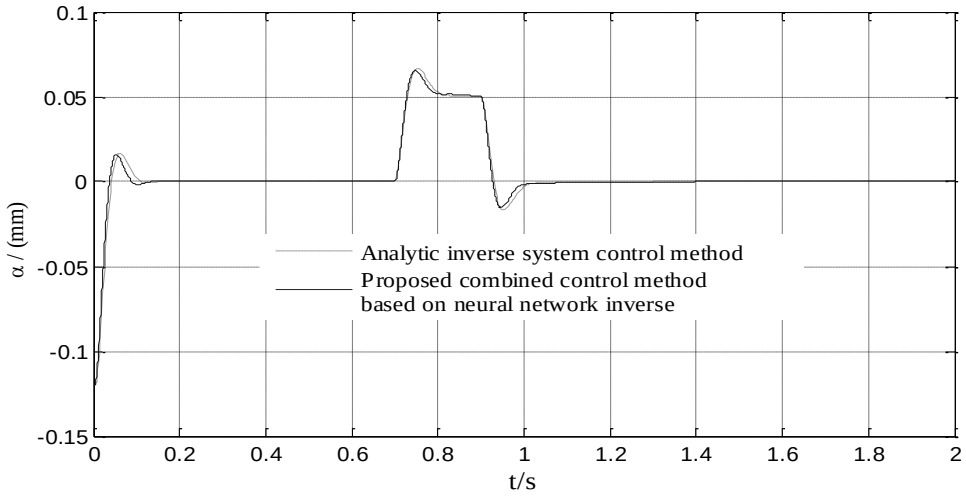

Figure 9. Response Curve of A Displacement Component

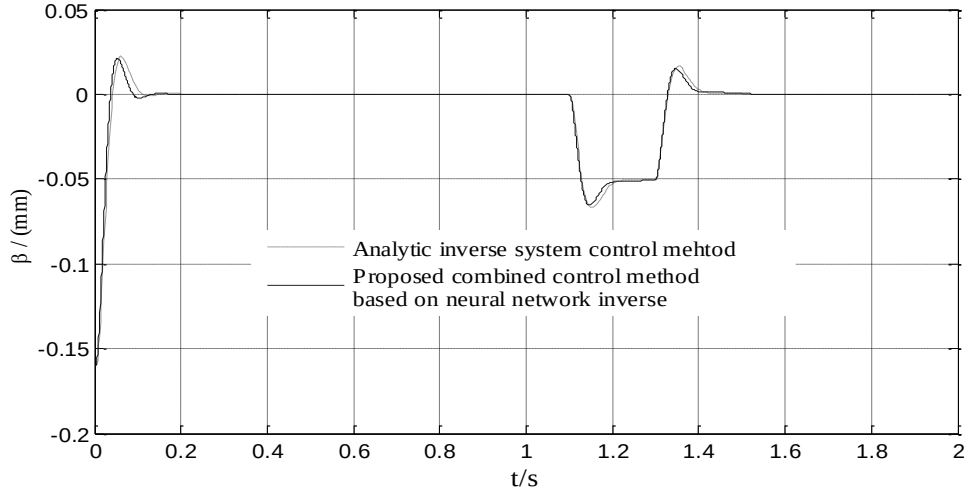

Figure 10. Response Curve of β Displacement Component

2) To verify the decoupling control performance, the given signal of rotor flux linkage is suddenly reduced to 0.6Wb at 0.3s, the given signal of motor speed is suddenly jumped to 2500r/min at 0.5s; the given signal of α displacement component is suddenly changed to 0.05mm at 0.7s and returned to zero at 1.1s; the given signal of β displacement component is suddenly changed to -0.05 mm at 0.8s and returned to zero at 1.3s. From Figure 7 ~ Figure 10: when the proposed combined control method is adopted, the change of one variable almost has no influence on other controllable variables; the transition process time of rotor flux linkage is shorter, the fluctuation amplitude of rotor flux linkage is obvious smaller. The simulation results shows that not only the decoupling control between motor speed, rotor flux linkage, and two displacement components can be achieved, but also higher response speed can be achieved.

3) To verify the ability of anti disturbance, the 8.0N.m torque load is added suddenly at 1.5s, and restored to zero at 1.7s. From Figure 8, in the sudden change process of torque load, the fluctuation of motor speed is less than 5r/min when the proposed combined control method is adopted; but the fluctuation of motor speed is about 15r/min when analytic inverse decoupling method is adopted. The simulation results have shown that the proposed combined control strategy owns higher ability of anti disturbance.

6. Conclusion

Aiming at the nonlinear and strong coupling problem of bearingless induction motor, a combined control strategy base on voltage control type neural network inverse system is proposed. On the basis of reversibility analysis of torque system that considers the stator current dynamics, the training sample sets are obtained from analytic inverse decoupling system; the initial weights and thresholds of BP neural network is optimized by genetic algorithms, after the static neural network is trained base LM algorithm, the neural network inverse model of torque system that considers stator current dynamics is achieved. By neural network inverse system, the torque system is decoupled into two second order subsystems, includes motor speed and rotor flux linkage subsystems. On the basis of this, according to the rotor flux linkage and stator current, the air gap flux linkage of torque system that is required in the magnetic suspension decoupling calculation, is acquired online; through the negative feedback closed loop control of radial displacement components and the compensation of unbalanced unilateral magnetic pull components, the given signals of controllable magnetic suspension force and its control current are acquired online. In the paper, for the stator voltage components of torque windings are selected as input variables, the current closed loop in original torque system can be omitted, and then the control system structure can be simplified to a certain extent.

From simulation results, based on the proposed combined control strategy, the decoupling control between rotor flux linkage, motor speed and two radial displacement components can be achieved; compared with the analytic inverse system decoupling control method, the control system owns better starting performance, quicker response speed, smaller overshoot, stronger ability of anti disturbance. The proposed combined control strategy is effective.

Acknowledgements

The supports of International Cooperation Project on Science and Technology of Henan Province (114300510029), National Natural Science Foundation of China (51277053), and Nature Science Fund of Henan Province Education Bureau (2010B510011), are acknowledged.

References

[1] J. Kriauciunas, R. Rinkeviciene and A. Baskys, "Self-Tuning Speed Controller of the Induction Motor Drive", Elektronika Ir Elektrotechnika, vol. 20, no. 6, **(2014)**, pp. 24-28.
[2] S.H. Kim, J.W. Shin and K. Ishiyama, "Magnetic Bearings and Synchronous Magnetic Axial Coupling for the Enhancement of the Driving Performance of Magnetic Wireless Pumps", IEEE Transactions on Magnetics, vol.50, no.1, **(2014)** pp.1-4.
[3] G. Barbaraci, G.V. Mariotti and A. Piscopo, "Active magnetic bearing design study", Journal of Vibration and Control, vol.19, no.16, **(2013)**, pp. 2491-2505.
[4] L. Zheng, "Combined Levitation Design and Control of a Novel M-DOF Actuator based on Air Bearing and Electromagnetic Principle", Elektronika Ir Elektrotechnika, vol. 19, no. 3, **(2013)**, pp. 27-32.
[5] W. Bu, S. Huang and S. Wan, "General analytical models of inductance matrices of four-pole bearingless motors with two-pole controlling windings", IEEE Transactions on Magnetics, vol.45, no.9, **(2009)**, pp.3316-3321.
[6] J. Huang, B. Li and H. Jiang, "Analysis and Control of Multiphase Permanent-Magnet Bearingless Motor with a Single Set of Half-Coiled Winding", IEEE Trans on Industrial Electronics, vol.61, no.7, **(2014)**, pp. 3137-3145.
[7] W. Bu, C. Zu, S. Wang and S. Huang, "Digital control system design and analyses of a 3- phase bearingless induction Motor", Turk J Elec Eng & Comp Sci, vol.22, no.5, **(2014)**, pp. 1193-1209.
[8] X.-L. Wang and P. He, "Stability analysis and verification for bearingless magnetic levitation system with disturbance rejection", Control Theory and Applications, vol.29, no.5, **(2012)**, pp. 665-672.
[9] R. Oishi, S. Horima and H. Sugimoto, "A Novel Parallel Motor Winding Structure for Bearingless Motors", IEEE Trans on Magn, vol.49, no.5, **(2013)**, pp. 2287-2290.

[10] W.-S. Bu, C.-L. Zu and C.-X. Lu, "Decoupling control strategy of bearingless induction motor under the conditions of considering current dynamic characteristics", Control Theory & Applications, vol.31, no.11, **(2014)**, pp. 1561-1567.
[11] Z. Wang, X. Liu and Y. Sun, "Nonlinear dynamic decoupling control for bearingless induction motor", China Mechanical Engineering, vol.23, no.8, **(2012)**, pp. 987-991.
[12] L. Dong, X. Liu and Y. Sun, "Decoupling control of the bearingless induction motor based on differential geometry variable-structure method", Proceedings of the 26th Chinese Control Conference, **(2007)**, vol.1, pp.17-21.
[13] H. Zhu, Y. Zhou and T. Li, "Decoupling control of 5 degrees of freedom bearingless induction motors using α-th order inverse system method", Acta Automatica Sinica, vol.33, no. 3, **(2007)**, pp.273-278.
[14] W.-S. Bu, C.-L. Zu and C.-X. Lu, "RFOC inverse dynamic decoupling control of bearingless induction motor", Electric Drive, vol.44, no.8, **(2014)**, pp.68-72.
[15] X. Sun and H. Zhu, "Decoupling Control of Bearingless Induction Motors Based on Neural Network Inverse System Method", Transactions of China Electrotechnical Society, vol.25, no.1, **(2010)**, pp. 43-49.
[16] Z.-Q. Wang and X.-X. Liu, "Nonlinear Internal Model Control for Bearingless Induction Motor",, ACTA Automatic Sinica, vol.39, no.4, **(2013)**, pp. 433-439.

